WM2016 Conference, March 6-10, 2016, Phoenix, Arizona, USA.

Effect of Feed Composition on Cold-Cap Formation in Laboratory-Scale Melter – 16336

Derek R. Dixon*, Michael J. Schweiger*, SeungMin Lee*, Jayven S. Heilman-Moore*, and Pavel Hrma*

*Pacific Northwest National Laboratory, Richland, WA 99354, derek.dixon@pnnl.gov

ABSTRACT

The development of advanced glass formulations is part of the plan for reducing the cost and time for treatment and vitrification of the 210,000 m^3 of nuclear waste at the Hanford Site in southeastern Washington State. One property of interest in this development is melt viscosity, which has a decisive influence on the rate of glass production. In an electric melter, the conversion process from feed-to-glass above the melt pool occurs in the cold cap. At the final stage of conversion, when the glass-forming melt becomes connected, gas-evolving reactions cause foaming. The transient melt viscosity affects foam stability. Three glasses were formulated with viscosities of 1.5, 3.5, and 9.5 Pa s at 1150°C by varying the SiO_2 content at the expense of B_2O_3, Li_2O, and Na_2O kept at constant proportions. Cold caps were produced by charging simulated high-alumina, high-level waste feeds in a laboratory-scale melter. The spread of the feed on the cold cap during charging and the cross-sectional structure of the final cold caps were compared. The amount of the foam and the size of the bubbles increased as the viscosity increased.

INTRODUCTION

The current plan for immobilizing the 210,000 m^3 of nuclear waste at the Hanford Site in southeastern Washington State is through vitrification into glass to take place in the Hanford Tank Waste Treatment and Immobilization Plant (WTP) [1, 2]. High-level waste (HLW) and low-activity waste will be vitrified in separate facilities [1]. Glass-forming and modifying additives are added to the separate waste streams before they are fed into electric melters operating at 1150°C [1].

The conversion process from waste feed to glass occurs in the cold cap above the melt pool. As the feed heats in the cold cap, glass-forming reactions ensue, causing the feed matrix to connect (>800°C) and trapping the reaction gases within the connected, transient melt to create a foam layer [3]. The gases accumulate into bubbles that eventually release through open pores in the feed or coalesce into cavities that travel horizontally and escape around the edges of the cold cap into the melter plenum space [4]. The foam layer restricts the heat transfer to the reacting feed, reducing the rate of melting [3, 4].

Glass viscosity is a function of both temperature and melt composition. Viscosity is allowed to vary in an electric melter with Inconel electrodes from 2 to 8 Pa s at the operating temperature, typically between 4 and 6 Pa s [5]. In the cold cap, the transient melt viscosity in the range 800°C to 1050°C affects the stability of the foam layer and has a significant influence on the rate of melting. Increasing the

rate of melting affects the glass production and may ultimately reduce the cost and shorten the life cycle of WTP cleanup [4]. However, few studies have attempted to characterize the transient melt viscosity during the feed-to-glass conversion in the temperature range from 100°C to 1150°C [6].

This study used feeds with different, known glass viscosities to observe the effect of compositional changes on both the foam layer of the cold cap and the movement of gas cavities in the glass melt around the cold cap. A volume expansion test examined the change in feed volume with respect to temperature and a laboratory-scale melter (LSM) allowed the feed spreading and gas bubbling to be observed during charging onto the cold cap.

EXPERIMENTAL METHODS

A19 Feed Composition

The HLW glass used in this study was adapted from the HWI-Al-19 with 45% waste loading formulation used in previous small-scale melter tests [7]. The adjusted composition, referred to here as A19, removed several of the trace oxides (BaO, CdO, K_2O, MgO, TiO_2, and ZnO), and the final A19 glass oxide composition is shown in TABLE I. The viscosity of the A19 glass at 1050°C and 1150°C was calculated using a nuclear waste glass viscosity mathematical model based on the glass composition (model 'B') [8], the results of which are shown in TABLE II.

Composition Variations

The amounts of B_2O_3, Li_2O, Na_2O, and SiO_2 in the A19 glass were varied to determine a glass composition with a calculated viscosity at 1050°C and 1150°C less than that calculated for A19 and a second glass with viscosity greater than A19. The compositions of the modified glasses at lower and higher viscosity (A19-1 and A19-9, respectively) are shown in TABLE I and the calculated viscosities are shown in TABLE II.

Viscosity Measurement

The A19, A19-1, and A19-9 glasses were batched separately by mixing the oxide feed chemicals (shown in TABLE I) to make 450 g of glass in an agate mill. The feed powders were melted at 1150°C for 1 hour, quenched, powdered, melted again at 1150°C for 1 hour, quenched, and broken into small pieces. Fifty cubic centimeters of glass were melted again at 1050°C and 1150°C and the viscosity was measured at both temperatures using a Brookfield[1] model DV-II viscometer with DilaSoft II[2] software for obtaining the data. The viscosity of each glass was determined from this data as previously described [6] and the results at each temperature for the glasses are shown in TABLE II as the measured values. Differences between the calculated and measured values for the glass viscosities

[1] Brookfield is a registered trademark of Brookfield Engineering.
[2] DilaSoft II is a registered trademark of Theta Industries, Inc.

can be attributed to multiple components of the A19 glasses (Al_2O_3 and B_2O_3) that approached the maximum mass fractions of the compositions used to create the viscosity model [8].

TABLE I. A19, A19-1, and A19-9 Glass Oxide Composition (Mass Fraction) and the Oxide Feed Components (g) for 1 g of Glass

Glass	A19-1	A19	A19-9	Oxide Feed	A19-1	A19	A19-9
Al_2O_3	0.2420	0.2420	0.2420	$Al(OH)_3$	0.3703	0.3703	0.3703
B_2O_3	0.2140	0.1919	0.1660	H_3BO_3	0.3801	0.3409	0.2949
Bi_2O_3	0.0116	0.0116	0.0116	Bi_2O_3	0.0116	0.0116	0.0116
CaO	0.0559	0.0559	0.0559	$CaCO_3$	0.0997	0.0997	0.0997
Cr_2O_3	0.0053	0.0053	0.0053	Cr_2O_3	0.0053	0.0053	0.0053
F	0.0067	0.0067	0.0067	NaF	0.0149	0.0149	0.0149
Fe_2O_3	0.0596	0.0596	0.0596	Fe_2O_3	0.0596	0.0596	0.0596
Li_2O	0.0398	0.0357	0.0309	Li_2CO_3	0.0985	0.0883	0.0764
Na_2O	0.1072	0.0961	0.0832	Na_2CO_3	0.1539	0.1350	0.1128
NiO	0.0040	0.0040	0.0040	NiO	0.0040	0.0040	0.0040
P_2O_5	0.0106	0.0106	0.0106	$NaPO_3$	0.0153	0.0153	0.0153
PbO	0.0041	0.0041	0.0041	PbO	0.0041	0.0041	0.0041
SiO_2	0.2332	0.2704	0.3141	SiO_2	0.2332	0.2704	0.3141
SO_3	0.0020	0.0020	0.0020	Na_2SO_4	0.0036	0.0036	0.0036
ZrO_2	0.0040	0.0040	0.0040	ZrO_2	0.0040	0.0040	0.0040
Sum	1.0000	1.0000	1.0000	Sum	1.4580	1.4270	1.3905

TABLE II. A19, A19-1, and A19-9 Glass Viscosities (Pa s)

	A19-1	A19	A19-9
1050°C (Calculated)	3.58	8.93	26.20
1050°C (Measured)	4.64	10.23	28.18
1150°C (Calculated)	1.49	3.49	9.48
1150°C (Measured)	1.94	3.64	8.49

Laboratory-Scale Melter Runs

For each glass composition, a slurry feed was batched with the feed chemicals (TABLE III) to make 250 g of glass added to deionized water up to a total volume of 500 mL to produce a final feed slurry concentration of 500 g L^{-1}. The silica source was crushed quartz of particle size ≤75 µm. The LSM was operated at 1200°C with 200 g of initial glass in the LSM crucible as described previously [9-12].

TABLE III. A19, A19-1, and A19-9 Slurry Feed Components (g) for 1 g of Glass

Slurry Feed	A19-1	A19	A19-9
$Al(OH)_3$	0.3718	0.3718	0.3718
H_3BO_3	0.3809	0.3416	0.2955
Bi_2O_3	0.0117	0.0117	0.0117
CaO	0.0109	0.0109	0.0109
$Cr_2O_3 \cdot 1.5H_2O$	0.0062	0.0062	0.0062
NaF	0.0150	0.0150	0.0150
$Fe(OH)_3$	0.0744	0.0744	0.0744
Li_2CO_3	0.0995	0.0892	0.0772
$Ni(OH)_2$	0.0050	0.0050	0.0050
$Fe(H_2PO_2)_3$	0.0125	0.0125	0.0125
PbO	0.0042	0.0042	0.0042
SiO_2	0.1910	0.2214	0.2572
Na_2SO_4	0.0036	0.0036	0.0036
$Zr(OH)_4$	0.0055	0.0055	0.0055
$CaSiO_3$	0.0971	0.0971	0.0971
NaOH	0.0199	0.0199	0.0199
Na_2CO_3	0.1188	0.1066	0.0922
$NaNO_2$	0.0035	0.0035	0.0035
$NaNO_3$	0.0124	0.0124	0.0124
$Na_2C_2O_4$	0.0013	0.0013	0.0013
Sum	1.4450	1.4137	1.3769

The first LSM run used the A19 slurry and varied the charging rate from 5.4 to 8.2 mL min^{-1} to determine an adequate charging rate that allowed for the formation of a cold cap with greater than 50% glass surface coverage and less than 100% coverage. The subsequent three runs used the A19, A19-1, and A19-9 feed slurries at a fixed charging rate of 6.5 mL min^{-1} for a run time of 35 minutes upon which the crucibles were removed from the LSM furnace and quenched on a copper block. Pictures and video were taken of the slurry spreading on the cold cap and gas bubbles bursting around the cold cap in 5 minute intervals from minute 5 to minute 30 of the runtime. After cooling, the cold caps from the final three runs were sectioned along existing fracture surfaces for optical imaging.

Volume Expansion Test

Powdered A19, A19-1, and A19-9 feeds, dried from slurry and using silica that was sieved to a particle size between 63 and 75 µm, were pressed into 13-mm diameter, 6-mm high pellets and heated at 10°C min^{-1} from room temperature to 1100°C. The expansion of each pellet was documented by photographing the

pellets at intervals through the heating process and the cross sectional area was determined by image analysis measurement. The volume of each pellet was calculated using a geometric approach [13-15], normalized by dividing by the initial pellet volume, and graphed against the temperature of the feed as shown in Fig. 1.

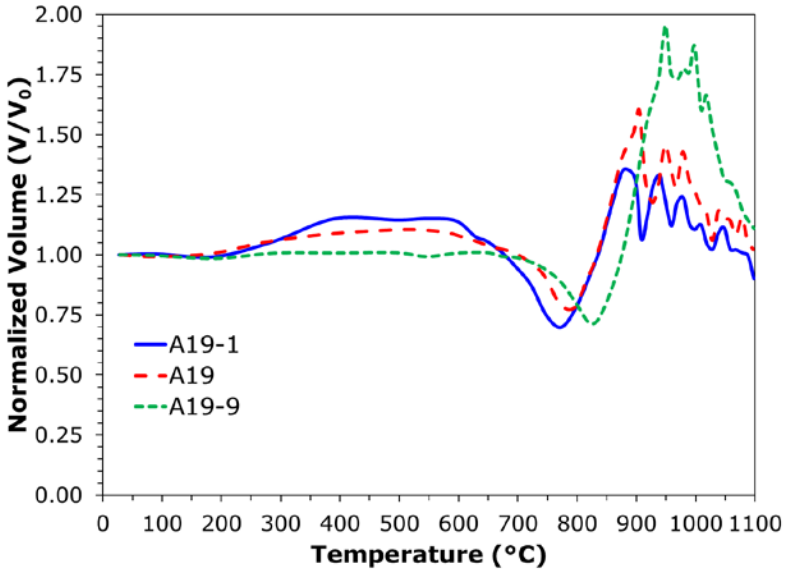

Fig. 1. Normalized volume expansion of A19, A19-1, and A19-9 feed pellets versus the temperature of the feed.

RESULTS AND DISCUSSION

The volume expansion of the feed pellets revealed that the point at which the volume reached a minimum occurred at higher temperatures for the feeds of increasing glass viscosity. At this point, the feed had begun to contract as the components connected to form a continuous, transient melt, but the gas produced from the glass-forming reactions had not begun to accumulate and expand the volume of the pellets. After this point, the volume of the pellets increased sharply as the gas became trapped by the transient melt. The maximum volume of the feed pellets, when the volume of gas trapped in the melt reached a maximum, increased for the feeds with increasing glass viscosity, indicating that the coalescing gases were forming larger bubbles in the pellet before bursting out of the surface.

During charging of the feeds in the LSM, gas cavities could be observed escaping around the edges of the cold cap as shown circled in Fig. 2a, b, and c. For the A19-1 run (Fig. 2a), the cavities were bursting frequently, but were small in size at ~0.5-1 cm diameter. In the A19 run (Fig. 2b), the cavities burst at a slightly decreased frequency as the A19-1, but they were slightly larger diameter, ~1-2 cm. Finally, for the A19-9 run (Fig. 2c), the cavities burst with much lower frequency and were larger, ~2-3 cm diameter. Overall, the size of the gas cavities that were released around the edges of the cold cap increased directly with glass viscosity while the frequency of cavities erupting decreased.

Cross sections of the quenched cold caps, split through the center, are shown in Fig. 2d, e, and f. While the glass cooled to 500°C in ~4 minutes, the cavities in the glass melt were able to merge around the edges of the cold caps and form larger void spaces. These void spaces became confined below the melt surface as the surface solidified and were observed in all of the cross sections. The deepest point of the A19-1 quenched cold cap was ~10 mm from the bottom of the crucible (marked in Fig. 2d), while in the A19 and A19-9 cold caps the point dipped ~4-5 mm from the bottom (denoted in Fig. 2e and Fig. 2f, respectively). In the A19-9 cold cap, the foam layer was ~1 cm thick, circled in Fig. 3 on a cross section from a fracture surface ~1 cm away from the center, but the foam layer was minimal (~0.2 cm) or not observed in the A19-1 or A19 cold caps.

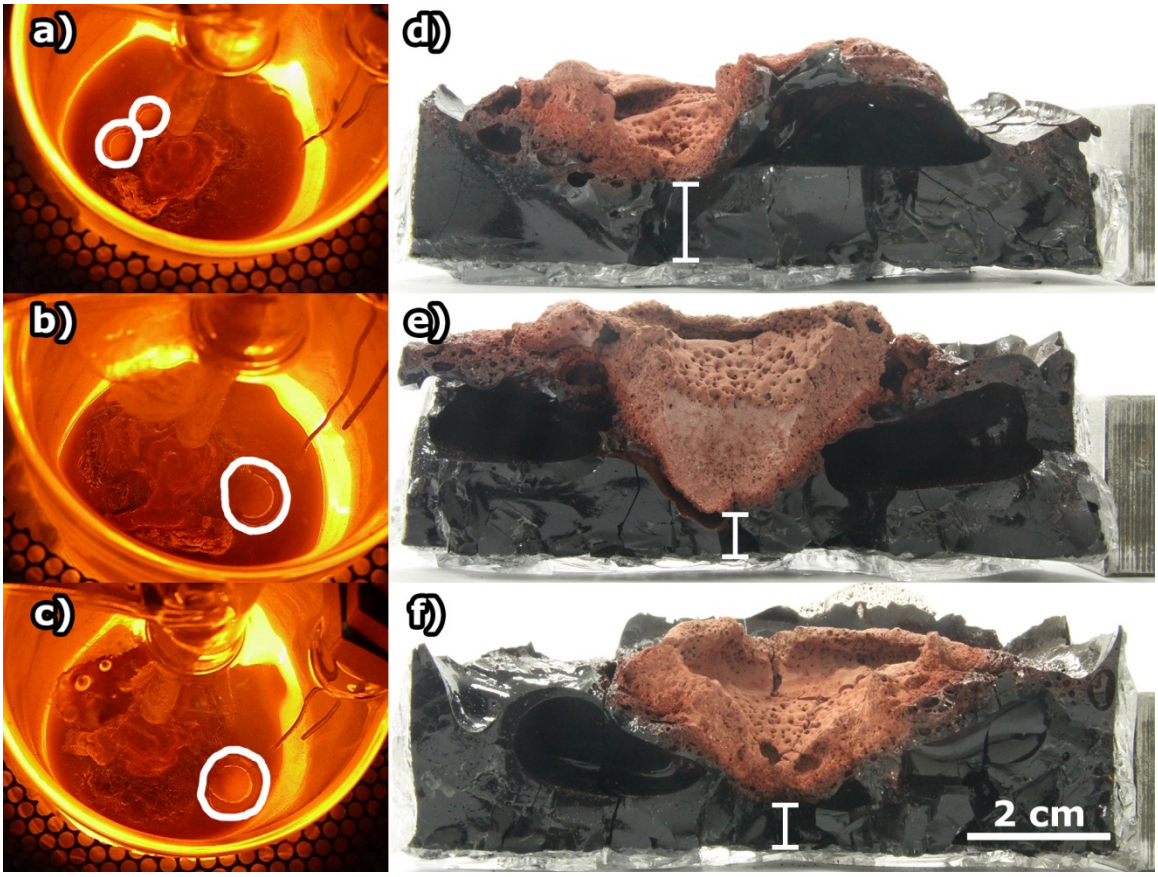

Fig. 2. a) A19-1, b) A19, and c) A19-9 cold caps during feed charging with cavities outlined. a, b, and c are not given on equivalent scales. Cross sections of LSM cold caps from d) A19-1, e) A19, and f) A19-9 feeds. The scale-bar is valid for d, e, and f.

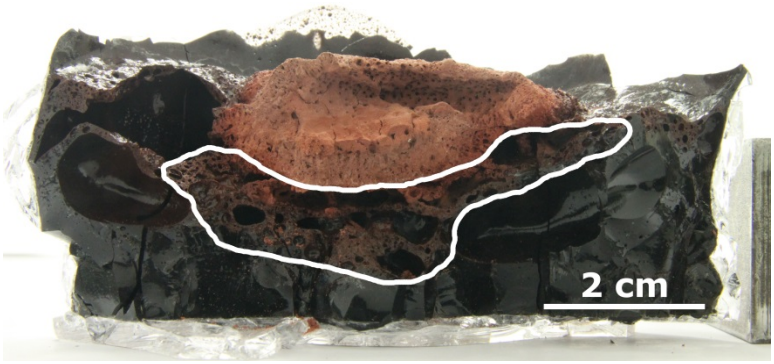

Fig. 3. Cross section of the A19-9 LSM cold cap with the foam layer outlined.

The results from the volume expansion test, observations of feed charging, and quenched cold caps all indicated that, as the viscosity of the glass increased, it was increasingly difficult for gas to escape the connected transient melt. In the foam layer of the cold cap, more bubbles were trapped by the more viscous glass compositions. As gas cavities traveled in the melt around the cold caps, the less viscous glass (A19-1) allowed small cavities to travel just under the cold cap and burst around the edges, while the higher viscosity glass (A19-9) caused more gas to coalesce and form larger cavities before breaking through the surface at lower frequency.

CONCLUSIONS

A high-aluminum HLW feed composition was modified to create three separate feeds with differing glass viscosities. The feeds were pressed into pellets for a volume expansion test and batched as slurries for charging into a LSM. The cold-cap formation and bubbling were observed in the LSM during slurry spreading and the structure of the cold caps were examined after quenching. More gas bubbles were trapped in the foam layer of the cold caps that were formed from compositions of increasing glass viscosity as demonstrated by the increasing size of pellet volume. Likewise, the cavities that escaped around the cold cap during melter charging increased in size, but decreased in frequency in the glass melts of greater viscosity.

REFERENCES

1. BECHTEL NATIONAL INC, "About The Project," http://www.hanfordvitplant.com/page/the-project/ (2015).
2. P.J. CERTA, P.A. EMPEY, M.N. WELLS, "River Protection Project System Plan," ORP-11242 Rev. 6, U.S. Department of Energy Office of River Protection, Richland, Washington (2011).
3. R. POKORNY, P. HRMA, "Model for the conversion of nuclear waste melter feed to glass," *Journal of Nuclear Materials*, **445**, 190-199 (2014).
4. R. POKORNY, Z. HILLIARD, D.R. DIXON, M.J. SCHWEIGER, D.P. GUILLEN, A.A. KRUGER, P. HRMA, “One-Dimensional Cold Cap Model for Melters with Bubblers,” *Journal of the American Ceramic Society*, **98**, 3112-3118 (2015).

5. J.D. VIENNA, D.-S. KIM, D.C. SKORSKI, J. MATYAS, “Glass Property Models and Constraints for Estimating the Glass to be Produced at Hanford by Implementing Current Advanced Glass Formulation Efforts,” PNNL-22631, Rev. 1, Pacific Northwest National Laboratory, Richland, WA (2013).
6. J. MARCIAL, J. CHUN, P. HRMA, M. SCHWEIGER, "Effect of Bubbles and Silica Dissolution on Melter Feed Rheology during Conversion to Glass," *Environmental Science & Technology*, **48**, 12173-12180 (2014).
7. K.S. MATLACK, W. KOT, I.L. PEGG, I. JOSEPH, A.A. KRUGER, “DM100 and DM1200 Melter Testing with High Waste Loading Glass Formulations for Hanford High-Aluminum HLW Streams, Test Plan 09T1690-1,” ORP-44198 Rev. 0, Vitreous State Laboratory, Washington, DC (2009).
8. P. HRMA, S.-S. HAN, “Effect of glass composition on activation energy of viscosity in glass-melting-temperature range,” *Journal of Non-Crystalline Solids*, **358**, 1818-1829 (2012).
9. D.R. DIXON, M.J. SCHWEIGER, B.J. RILEY, R. POKORNY, P. HRMA, “Temperature Distribution within a Cold Cap during Nuclear Waste Vitrification,” *Environmental Science & Technology*, **49**, 8856-8863 (2015).
10. D.R. DIXON, M.J. SCHWEIGER, B.J. RILEY, R. POKORNY, P. HRMA, “Cold-Cap Temperature Profile Comparison between the Laboratory and Mathematical Model,” *WM2015 Conference*, Paper#15591, Phoenix, AZ (2015).
11. D.R. DIXON, M.J. SCHWEIGER, P. HRMA, "Characterizing a High-Level Waste Cold Cap via Elemental and Structural Configuration," *WM2014 Conference*, Paper#14185, Phoenix, AZ (2014).
12. D.R. DIXON, M.J. SCHWEIGER, P. HRMA, "Effect of Feeding Rate on the Cold Cap Configuration in a Laboratory-Scale Melter," *WM2013 Conference*, Paper#13362, Phoenix, AZ (2013).
13. Z. HILLIARD, P. HRMA, “A Method for Determining Bulk Density, Material Density, and Porosity of Melter Feed During Nuclear Waste Vitrification,” *Journal of the American Ceramic Society*, (2015).
14. S. LEE, Z. HILLIARD, J.S. HEILMAN-MOORE, D.R. DIXON, P. HRMA, M.J. SCHWEIGER, “The Effect of Quartz Particle Size and Melt Viscosity on HLW Melter Feed Pellet Test Response,” *WM2016 Conference*, Paper#16226, Phoenix, AZ (2016).
15. B.J. VANDERVEER, Z.J. HILLIARD, P. HRMA, D.K. PEELER, M.J. SCHWEIGER, “Comparison of High-Level Waste Glass Feeds Containing Frit and Glass Forming Chemicals,” *WM2016 Conference*, Paper#16154, Phoenix, AZ (2016).

ACKNOWLEDGEMENTS

This work was supported by the U.S. Department of Energy’s Waste Treatment and Immobilization Plant Federal Project Office under the direction of Dr. Albert A. Kruger. The Pacific Northwest National Laboratory is operated for the Department of Energy by Battelle Memorial Institute under contract DE AC05 76RL0 1830. The authors would like to thank David Peeler for his discussion about the WTP and advanced glass formulations and Richard Pokorny for his discussion about the cold-cap foam layer.